

Luminescence Spectra of a Quantum-Dot Cascade Laser

Vadim Apalkov and Tapash Chakraborty

Max-Planck-Institut für Physik Komplexer Systeme, 01187 Dresden, Germany

A quantum cascade laser where the quantum wells in the active regions are replaced by quantum dots with their atom-like discrete energy levels is an interesting system to study novel features in optical spectroscopy. We study structures suitable for diagonal lasing transitions in coupled dots, and vertical lasing transitions in a single dot, in the active regions of the laser device. The luminescence spectra as a function of electron number and dot size show that for diagonal transitions, a significant amount of blue-shift in the emission spectra can be achieved by increasing electron population in the quantum dots as well as by decreasing the size of the dots.

Ever since the original work on quantum cascade laser (QCL) by Faist et al. [1,2] in 1994, the unipolar semiconductor laser based on intersubband transitions in coupled quantum wells have undergone rapid developments. QCLs created in InGaAs/AlInAs systems have achieved record high power outputs in the mid-infrared range that has the potential for wide-ranging applications [3,4]. Applications, often mentioned in the literature, are in environmental sensing, pollution monitoring, medical diagnostics, etc. QCLs in other material systems [5–7] have also shown promise for improved performance.

In this work, we study the optical properties of quantum cascade lasers where the quantum wells in the active regions are replaced by quantum dots (QD). The latter objects, popularly known as artificial atoms [8], where the electron motion is quantized in all three spatial directions, have been receiving much attention. These zero-dimensional quantum confined systems are useful for investigating the fundamental concepts of nanostructures [8,9] as well as for its application potentials. In recent years, there has been considerable progress in quantum-dot laser research [10]. Because of their discrete atom-like states, quantum-dot lasers are expected to have better performance than the quantum-well lasers [11,12]. Developments of self-organizing growth techniques that allow formation of high-density of quantum dots with nanometer dimensions rapidly enhanced the development of QD-laser research, where the performance is now comparable to that of quantum-well lasers [13,14]. Researchers have also found important applications of quantum dots in storage devices [15,16] and fluorescence markers [17].

Here we combine the properties of these two very interesting nanostructures, the QCLs and the QDs, to explore the luminescence spectra of a quantum-dot cascade laser. There has been already some suggestions in the literature that quantum-dot cascade lasers will significantly reduce the threshold current density by eliminating single phonon decays [18,19]. This prediction was based on the fact that quantization of electron motion in the plane would greatly inhibit single phonon decay, provided the dots are sufficiently small. There is however no report in the literature (theoretical or experimental) as yet, on the physical properties of a quantum-dot cascade laser. In this work, we have explored the luminescence spectra of quantum cascade lasers, both for vertical as well as diagonal

lasing transitions, for various values of the dot size and number of electrons in the quantum dots. One advantage of the quantum-dot cascade laser for theoretical studies over the quantum-well cascade laser is that, for few electrons in the QD, most of the physical properties can be calculated exactly, albeit numerically [8].

The single-electron Hamiltonian for our system is

$$\mathcal{H}' = \frac{p_x^2}{2m^*} + \frac{p_y^2}{2m^*} + V_{\text{plane}}(x, y) + \frac{p_z^2}{2m^*} + V_{\text{conf}}(z) \quad (1)$$

where the confinement potential in the z -direction [Fig. 1] is

$$V_{\text{conf}}(z) = -eFz + \begin{cases} 0 & \text{for wells} \\ U_0 & \text{for barriers} \end{cases}$$

with F being the electric field in the z -direction. The confinement potential in the xy -plane is

$$V_{\text{plane}}(x, y) = \begin{cases} 0 & |x| < L/2 \text{ and } |y| < L/2 \\ U_0 & \text{otherwise.} \end{cases}$$

The eigenfunctions and eigenvalues of the single-electron Hamiltonian [1] is obtained from

$$\psi_{nmk} = \varphi_{n,k}(x)\varphi_{m,k}(y)\chi_k(z)$$

where

$$\left[\frac{p_x^2}{2m^*} + V_{\text{plane}}(x) \right] \varphi_{n,k}(x) = E_n \varphi_{n,k}(x) \quad (2)$$

$$\left[\frac{p_z^2}{2m^*} + V_{\text{conf}}(z) \right] \chi_k(z) = \tilde{E}_k \chi_k(z) \quad (3)$$

$$E_{nmk} = E_{n,k} + E_{m,k} + \tilde{E}_k.$$

Because of the band nonparabolicity the electron mass depends on the total energy $m^*(E_{nmk})$ [20]. In our calculations that follow, we consider only two subbands in the z -direction ($k = 1, 2$) and for a given k all possible states in the xy -plane with the condition, $E_{nmk} < U_0$.

The solutions of Eq. (2) are usual cos (sin)-type

$$\varphi_{n,k}(x) = \mathcal{N} \begin{cases} \begin{cases} \cos \left(\sqrt{2m_w E_n L/2} \right) \\ \sin \left(\sqrt{2m_w E_n L/2} \right) \end{cases} \\ \times e^{-\sqrt{2m_b(U_0-E_n)}(X-L/2)}, & x > L/2 \\ \begin{cases} \cos \left(\sqrt{2m_w E_n x} \right) \\ \sin \left(\sqrt{2m_w E_n x} \right) \end{cases}, & |x| < L/2 \\ \begin{cases} \cos \left(\sqrt{2m_w E_n L/2} \right) \\ -\sin \left(\sqrt{2m_w E_n L/2} \right) \end{cases} \\ \times e^{-\sqrt{2m_b(U_0-E_n)}(X+L/2)}, & x < -L/2 \end{cases}$$

where $m_w(m_b)$ is the electron effective mass in the well (barrier). The energy E_n was calculated numerically from

$$\tan \kappa = \sqrt{\frac{m_w}{m_b}} \sqrt{\frac{\gamma^2 - \kappa^2}{\kappa^2}}, \quad \text{for even solutions}$$

$$\tan \kappa = -\sqrt{\frac{m_b}{m_w}} \sqrt{\frac{\kappa^2}{\gamma^2 - \kappa^2}}, \quad \text{for odd solutions}$$

where $\kappa^2 = E_n \frac{L^2}{2} m_w$, $\gamma^2 = U_0 \frac{L^2}{2} m_w$. Solutions of Eq. (3) are obtained numerically for the two lowest states (subbands) shown in Fig. 1. Due to the $x \leftrightarrow y$ symmetry, some of the levels are two-fold degenerate (for example, $E_{122} = E_{212}$).

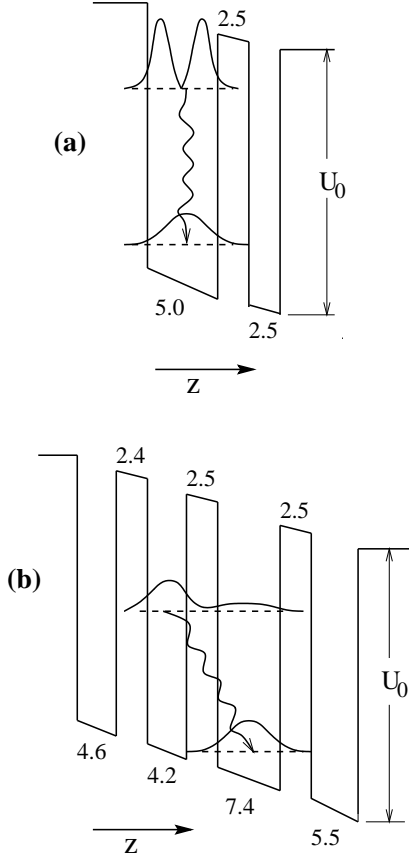


FIG. 1. Energy band diagram (schematic) of the active region of a quantum cascade laser structure and (a) vertical lasing transition under an average applied electric field of 85 kV/cm and (b) diagonal transition under a field of 55 kV/cm. The relevant wave functions (moduli squared) as well as the transition corresponding to the laser action are also shown schematically. The numbers (in nm) are the well ($\text{Ga}_{0.47}\text{In}_{0.53}\text{As}$) and barrier ($\text{Al}_{0.48}\text{In}_{0.52}\text{As}$) widths. For vertical transitions, these parameters are taken from [18]. Material parameters considered in this work are: electron effective mass m_e^* ($\text{Ga}_{0.47}\text{In}_{0.53}\text{As}$)= $0.043 m_0$, m_e^* ($\text{Al}_{0.48}\text{In}_{0.52}\text{As}$)= $0.078 m_0$, the conduction band discontinuity, $U_0 = 520$ meV, the nonparabolicity coefficient, $\gamma_w = 1.3 \times 10^{-18} \text{ m}^2$ for the well and $\gamma_b = 0.39 \times 10^{-18} \text{ m}^2$ for the barrier.

From the single-electron basis functions, we construct the N -electron basis

$$\Phi_{n_i m_i k_i}(\mathbf{r}_1, \dots, \mathbf{r}_N)$$

$$= \mathcal{A} \psi_{n_1 m_1 k_1}(\mathbf{r}_1) \sigma_1 \cdots \psi_{n_N m_N k_N}(\mathbf{r}_N) \sigma_N \quad (4)$$

where, as usual, σ_i is the spin part of the wave function [$\sigma_i = \begin{pmatrix} 1 \\ 0 \end{pmatrix}$ or $\begin{pmatrix} 0 \\ 1 \end{pmatrix}$] and \mathcal{A} is the antisymmetrization operator. The total many-electron Hamiltonian is written as

$$\mathcal{H} = \sum_{i=1}^N \mathcal{H}'_i + \sum_{i < j}^N V(|\mathbf{r}_i - \mathbf{r}_j|) \quad (5)$$

where \mathcal{H}' is given by Eq. (1). For inter-electron interactions we consider the Coulomb interaction

$$V(|\mathbf{r}_i - \mathbf{r}_j|) = \frac{e^2}{\epsilon |\mathbf{r}_i - \mathbf{r}_j|}. \quad (6)$$

The Hamiltonian matrix is then calculated in the basis (4). The single-electron Hamiltonian has only diagonal contribution while the interaction term gives non-diagonal contributions

$$\langle n_{i_1} m_{i_1} k_{i_1}; n_{i_2} m_{i_2} k_{i_2} | V | n_{j_1} m_{j_1} k_{j_1}; n_{j_2} m_{j_2} k_{j_2} \rangle$$

$$= \text{Tr}_\sigma \int d\mathbf{r}_1 d\mathbf{r}_2 \mathcal{A} \left[\Psi_{n_{i_1} m_{i_1} k_{i_1}}^*(\mathbf{r}_1) \sigma_{i_1} \Psi_{n_{i_2} m_{i_2} k_{i_2}}^*(\mathbf{r}_2) \sigma_{i_2} \right]$$

$$\times V(|\mathbf{r}_1 - \mathbf{r}_2|) \mathcal{A} \left[\Psi_{n_{j_1} m_{j_1} k_{j_1}}^*(\mathbf{r}_2) \sigma_{j_1} \Psi_{n_{j_2} m_{j_2} k_{j_2}}^*(\mathbf{r}_1) \sigma_{j_2} \right].$$

The eigenvalues and eigenfunctions were calculated by exact (numerical) diagonalization of the Hamiltonian matrix. As the many-body Hamiltonian also has the $x \leftrightarrow y$ symmetry some of the states are two-fold degenerate.

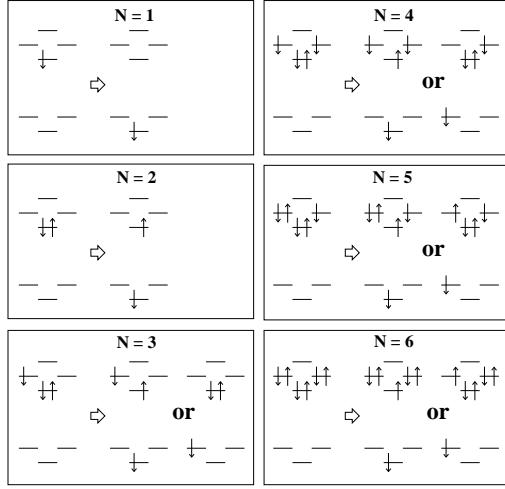


FIG. 2. Energy levels and spin configurations and the allowed optical transitions (schematic) for quantum dots with noninteracting electrons. Here, \uparrow denotes electrons with spin up and \downarrow that for spin down.

In the initial state (before optical emission) all the electrons are in the second subband, $k = 2$. In the final state (after optical emission) one electron is in the first subband, $k = 1$, and all other electrons are in the second subband, $k = 2$. The intensity of optical transitions is found from the expression

$$\mathcal{I}_{if}(\omega) = \frac{1}{Z} \sum_{if} \delta(\omega - E_i + E_f) \left| \int \chi_1(z) z \chi_2(z) dz \int \Phi_i^*(x_1 y_1, \dots, x_N y_N) \times \Phi_f(x_1 y_1, \dots, x_N y_N) dx_1 dy_1 \dots dx_N dy_N \right|^2 \times \exp(-\beta E_i)$$

where $Z = \sum_i e^{-\beta E_i}$ is the partition function and $\beta = 1/kT$. In all our computation, we take $T = 20$ K.

The energy levels and possible optical transitions for the noninteracting systems are sketched in Fig. 2. Clearly, there are two types of transitions for the noninteracting electron system: (a) from the one-particle ground state of the second subband to the one-particle ground state of the first subband and, (b) from the one-particle excited state of the second subband to the one-particle excited state of the first subband. These are the transitions between states with same quantum number in the xy -plane. Energies of these transitions are different due to band nonparabolicity. The nonparabolicity can also allow transitions between states with different quantum numbers in the xy -plane but the intensity of these transitions are very small because the nonparabolicity

has small effect on the electron wave functions. Therefore, we can safely assume that the optical transitions are allowed only between the states with the same quantum numbers in the xy -plane. One also notices from Fig. 2 that optical transitions to the ground state of the final noninteracting system are forbidden for $N > 2$.

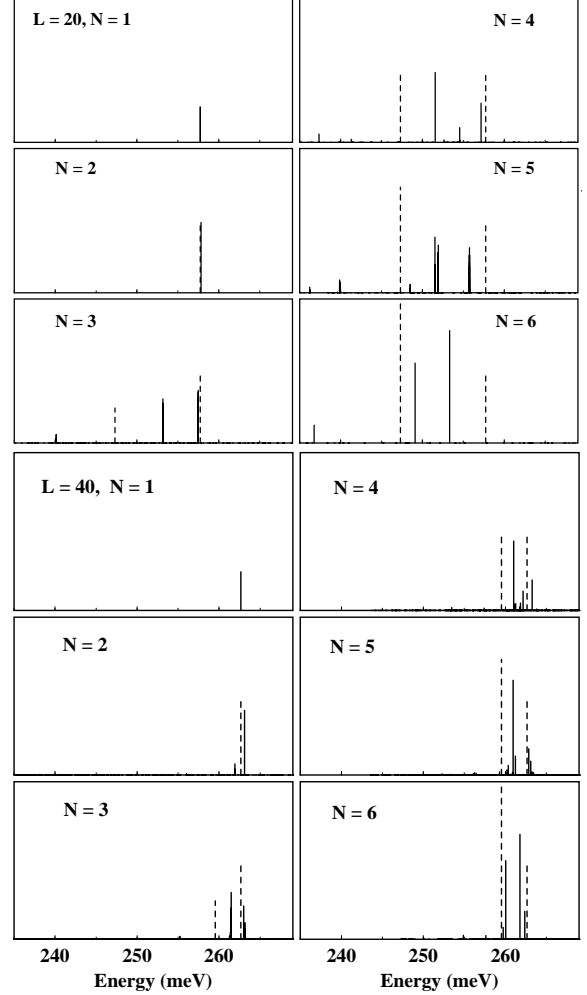


FIG. 3. Luminescence spectra of a quantum-dot cascade laser and *vertical* optical transitions for various values of the dot size (L in nm) and number of electrons (N) in the dot. The dashed lines correspond to luminescence of noninteracting electron systems.

In Fig. 3, the optical spectra is shown for vertical transitions [Fig. 1(a)] and for two sizes of quantum dots: $L = 20$ nm and $L = 40$ nm, and for different numbers of electrons in the quantum dot. In all these cases the first moment of the emission spectra for the interacting system is almost the same as that for the noninteracting system. This is because in the case of vertical transitions the Coulomb interaction between the electrons in the second subband and those in the second and the first sub-

bands are almost the same (electrons are localized in the same quantum well in the z -direction). The Coulomb interaction between electrons is about half the energy separation between the one-electron states in the xy -plane for $L = 20$ nm and is of the same order as the energy separation between xy levels in $L = 40$ nm. That is why the interaction is more important for $L = 40$ nm. For the two electron system there is a small blue-shift of the emission line due to the interaction which increases with an increase of the size of the quantum well. In addition, there is also a small red satellite at $L = 40$ nm. For the six-electron system, the interaction results in redistribution of the intensities between peaks: the higher energy peak becomes more intense than that for the lower energy. For 3,4 and 5 electrons in a noninteracting system, we have a degenerate initial state. The degeneracy is lifted by the interaction and for the four electron system the initial ground state is partially polarized as expected from Hund's rules. The interaction also results in the appearance of satellites and at the same time the separation between the main peaks becomes smaller for the interacting system than for the noninteracting case.

In Fig. 4 the optical spectra is presented for diagonal optical transitions [Fig. 1 (b)] and for two sizes of quantum dots: $L = 10$ nm and $L = 20$ nm, and for different numbers of electrons. Interestingly, we notice the behavior characteristics of fully filled shells for 2 and 6 electrons. The Coulomb interaction is about two times smaller than the separations between shell levels in the xy -plane for $L = 20$ nm and about six times smaller for $L = 10$ nm. For the two-electron system, we have a single line for both non-interacting and interacting systems. For the six-electron system and $L = 10$ nm, the emission spectra has the same two-peak structure as for the noninteraction system. For $L = 10$ nm there is a small redistribution of intensities between the peaks while there is an additional line for $L = 20$ nm. For 2,3 and 4 electrons in the dot, the interaction results in splitting of lines of the corresponding noninteracting systems. With increasing size of the quantum dots the lower energy lines become more intense.

As the Coulomb interaction between electrons in the second subband is about two times larger than the Coulomb interaction between electrons in the second and in the first subband we have a highly non-symmetric system and as a result there is the *large blue shift* in all cases, compared to the noninteracting system. This blue shift decreases with increasing size of the quantum dots. Further, the blue shift increases with increasing number of electrons. For $L = 10$ nm, there is a blue shift of the emission line of about 55 meV when the electron number is increased from 1 to 6.

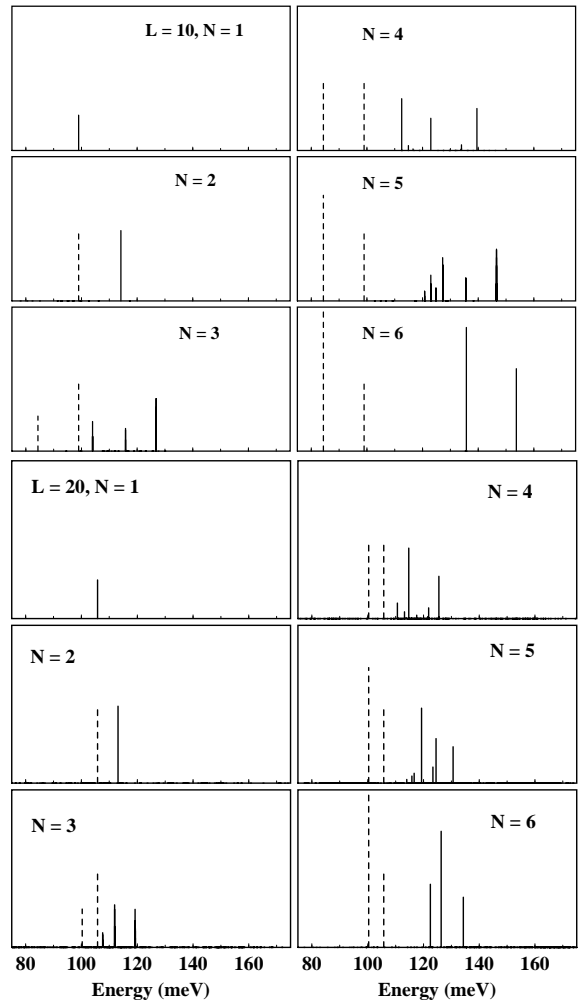


FIG. 4. Luminescence spectra of a quantum-dot cascade laser and *diagonal* optical transitions for various values of the dot size (L in nm) and number of electrons (N) in the dot. The dashed lines correspond to luminescence of noninteracting electron systems.

In summary, we have studied the luminescence spectra of a quantum-dot cascade laser suitable for vertical or diagonal transitions. The spectra as a function of the dot size and electron numbers in the dot reflect the atom-like character due to the presence of quantum dots. Most interestingly, significant amount of blue-shift in the emission spectra can be achieved by increasing electron population in the quantum dots as well as by decreasing the size of the dots. This is most clearly seen for the diagonal transitions. This opens up the possibility of tuning the laser emission frequency for diagonal transitions by changing the number of electrons in quantum dots and/or decreasing the size of the dots.

We thank P. Fulde for his support and kind hospitality in Dresden.

- [1] J. Faist et al., *Science* **264**, 553 (1994).
- [2] J. Faist et al., *Appl. Phys. Lett.* **66**, 538 (1995).
- [3] J. Faist et al., *IEEE Photon. Technol. Lett.* **10**, 1100 (1998).
- [4] F. Capasso et al., *Opt. Photonics News* **10**, 31 (1999).
- [5] R.Q. Yang et al., *Appl. Phys. Lett.* **71**, 2409 (1997).
- [6] C. Sirtori et al., *Appl. Phys. Lett.* **73**, 3486 (1998).
- [7] Proceedings of the Fifth International Conference on Intersubband Transitions in Quantum Wells, editors, M. Helm, K. Unterrainer, *Physica E* **7** (2000).
- [8] T. Chakraborty, *Quantum Dots* (North-Holland, Amsterdam, 1999).
- [9] S. Tarucha, et al., *Jpn. J. Appl. Phys.* **36**, 3917 (1997).
- [10] M. Grundmann, *Physica E* **5**, 167 (2000).
- [11] Y. Arakawa, H. Sakaki, *Appl. Phys. Lett.* **40**, 939 (1982).
- [12] K.J. Vahala, *IEEE J. Quantum Electron.* **24**, 523 (1988).
- [13] Y.M. Manz, O.G. Schmidt, K. Eberl, *Appl. Phys. Lett.* **76**, 3343 (2000).
- [14] K. Mukai, et al., *Appl. Phys. Lett.* **76**, 3349 (2000).
- [15] J.J. Finley, et al., *Appl. Phys. Lett.* **73**, 2628 (1998).
- [16] T. Lundström, et al., *Science* **286**, 2312 (1999).
- [17] M. Bruchez, Jr., et al., *Science* **281**, 2013 (1998).
- [18] C.F. Hsu et al., *SPIE* **3001**, 271-281 (1997).
- [19] N.S. Wingreen, C.A. Stafford, *IEEE J. Quantum Electron.* **33**, 1170 (1997).
- [20] In our calculations that follow, we consider only the main contribution due to \tilde{E}_k , i.e., the mass depends only on \tilde{E}_k (both in Eq. [2] and [3]). This approximation simplifies the analysis but will only result in small changes in the final energies.